



## Deletion of the X-linked opsin gene array locus control region (LCR) results in disruption of the cone mosaic

Joseph Carroll<sup>a,b,c,\*</sup>, Ethan A. Rossi<sup>d,1</sup>, Jason Porter<sup>e</sup>, Jay Neitz<sup>f</sup>, Austin Roorda<sup>d</sup>, David R. Williams<sup>g</sup>, Maureen Neitz<sup>f</sup>

<sup>a</sup> Department of Ophthalmology, Medical College of Wisconsin, Milwaukee, WI 53226, United States

<sup>b</sup> Department of Cell Biology, Neurobiology & Anatomy, Medical College of Wisconsin, Milwaukee, WI 53226, United States

<sup>c</sup> Department of Biophysics, Medical College of Wisconsin, Milwaukee, WI 53226, United States

<sup>d</sup> School of Optometry, University of California Berkeley, Berkeley, CA 94720, United States

<sup>e</sup> College of Optometry, University of Houston, Houston, TX 77204, United States

<sup>f</sup> Department of Ophthalmology, University of Washington, Seattle, WA 98195, United States

<sup>g</sup> Center for Visual Science, University of Rochester, Rochester, NY 14627, United States

### ARTICLE INFO

#### Article history:

Received 26 May 2010

Received in revised form 7 July 2010

#### Keywords:

Adaptive optics

Blue cone monochromacy

Color vision

Cones

Opsin

Photopigment

### ABSTRACT

Blue cone monochromacy (BCM) is an X-linked condition in which long- (L) and middle- (M) wavelength-sensitive cone function is absent. Due to the X-linked nature of the condition, female carriers are spared from a full manifestation of the associated defects but can show visual symptoms, including abnormal cone electroretinograms. Here we imaged the cone mosaic in four females carrying an L/M array with deletion of the locus control region, resulting in an absence of L/M opsin gene expression (effectively acting as a cone opsin knockout). On average, they had cone mosaics with reduced density and disrupted organization compared to normal trichromats. This suggests that the absence of opsin in a subset of cones results in their early degeneration, with X-inactivation the likely mechanism underlying phenotypic variability in BCM carriers.

© 2010 Elsevier Ltd. All rights reserved.

### 1. Introduction

Blue cone monochromacy (BCM; MIM303700) is an X-linked condition affecting approximately 1 in 100,000 individuals, and is characterized by an absence of both long- (L) and middle- (M) wavelength-sensitive cone function. There are two main genetic causes of BCM, sometimes referred to as one-step or two-step mutations (Nathans et al., 1989, 1993). *One-step mutations* involve a deletion of the X-chromosome opsin locus control region (LCR), which has been shown to be required for normal transcription of the L and M pigment genes (Nathans et al., 1989; Smallwood, Wang, & Nathans, 2002; Wang et al., 1999). *Two-step mutations* involve a deletion of all but one of the X-chromosome visual pigment genes and the remaining gene in the array encodes a non-func-

tional pigment. There is considerable variation within the two-step pathway (Ayyagari et al., 2000; Gardner et al., 2009; Ladekjaer-Mikkelsen, Rosenberg, & Jørgensen, 1996; Nathans et al., 1993). In both mutational pathways, affected individuals have poor acuity, myopia, nystagmus, and minimally detectable cone-mediated electroretinogram (ERG) responses. Female carriers appear to be spared from a full manifestation of the associated defects, but can show abnormal cone ERG responses (Berson, Sandberg, Maguire, Bromley, & Roderick, 1986; Spivey, Pearlman, & Burian, 1964) and eye movement defects (Gottlob, 1994). There have also been reports of pigmentary maculopathy in some BCM carriers (Ayyagari, Kakuk, et al., 1999), but this has not been definitively linked to their condition.

Little is known about the consequence of the lack of cone opsin on the structure of the cone mosaic. Based on experiments in mice, it was shown that the absence of rhodopsin in the  $Rho^{-/-}$  mouse results in a failure of the rod outer segment to form and ultimately leads to complete photoreceptor degeneration (Humphries et al., 1997). Recent work suggests that the absence of normal rhodopsin prevents disc biogenesis (Gross et al., 2006). While *in vivo* work in humans has shown that expression of a mutant cone opsin can affect the function and structural integrity of the associated cone photoreceptor (Carroll et al., 2009; Carroll, Neitz, Hofer, Neitz, &

*Abbreviations:* BCM, blue cone monochromacy; ERG, electroretinogram; AO, adaptive optics; AOSLO, adaptive optics scanning laser ophthalmoscope; LCR, locus control region.

\* Corresponding author. Address: Department of Ophthalmology, Medical College of Wisconsin, 925 N87th Street, Milwaukee, WI 53226, United States. Fax: +1 414 456 6690.

E-mail address: [jcarroll@mcw.edu](mailto:jcarroll@mcw.edu) (J. Carroll).

<sup>1</sup> These authors contributed equally to this work.

Williams, 2004; Torti et al., 2009), it is not known how the absence of cone opsin affects cone structure. Affected BCM males can show substantial retinal degeneration, which could make *in vivo* assessment of cone structure difficult. However in female carriers of BCM, on average, half of the photoreceptors fated to be L or M cones will fail to make photopigment, due to the process of X-inactivation. By examining the integrity of the cone mosaic, these BCM carriers provide an interesting model with which to examine how the absence of opsin affects the viability of the associated cone photoreceptors.

Here we imaged six females from two families with multiple males manifesting BCM. Through a comprehensive molecular analysis, we were able to determine that the BCM phenotype in both families was caused by a deletion encompassing the LCR (a one-step mutation). One female was an obligate carrier, and we determined carrier status using molecular analysis in three of the remaining five females. Using adaptive optics (AO), we obtained images of the cone mosaic and found that the number of visible cones was significantly reduced and the regularity of the cone mosaic was disrupted compared to normals. These imaging data suggest that failure to express opsin results in the early degeneration of the associated cone photoreceptor.

## 2. Methods

### 2.1. Subject selection

Subjects provided informed consent after the nature and possible consequences of the study were explained. All research adhered to the tenets of the Declaration of Helsinki, and study protocols were approved by institutional research boards at the University of Rochester, Medical College of Wisconsin, and University of California Berkeley. We studied two unrelated families with multiple males affected with BCM, and pedigrees of both families are shown in Fig. 1. Family B was discovered to belong to a larger pedigree originally reported by Berson et al. (1986). From these families, we recruited five women of unknown carrier status and a single obligate carrier to participate in retinal imaging studies to assess the integrity of the cone photoreceptor mosaic. The women of unknown carrier status participated in genetic studies to determine carrier status. Color vision was assessed using a variety of tests, including the Rayleigh match, pseudoisochromatic plates (AO-HRR, Dvorine, and Ishihara), and the Farnsworth-Munsell 100-Hue Test. All six women performed normally on these tests. Complete ophthalmic exams on these six women revealed no retinal abnormalities, except for subtle RPE pigment mottling in the two oldest females (Family A, III-8 and Family B, IV-7). Fourteen unrelated subjects with normal color vision and no visible retinal pathology were recruited for retinal imaging studies. To aid in the mapping of the genetic cause of BCM in each family, three affected males, one unaffected male, and two obligate carriers were recruited from within the families for the genetic studies (see Section 2.2.1).

### 2.2. Genetic analysis

#### 2.2.1. Subjects

The pedigrees of the two families examined are shown in Fig. 1, with each subject for whom we obtained a blood sample marked with an asterisk. Genomic DNA was isolated from whole blood. We conducted genetic analyses on DNA from two brothers from Family A (III-5 and III-7), their sister (III-8), and her daughter (IV-6). For Family B, we conducted genetic analyses on three affected males (IV-9, V-5, and VI-2), and three sisters of V-5 (V-2, V-4, and V-6). In addition we analyzed DNA from two obligate carriers

in the family – V-10, who is the daughter of IV-9 and mother of VI-2, and III-6, who is the grandmother of affected male V-5.

At the time of analysis, the carrier status for subjects III-8 and IV-6 (Family A) and V-2, V-4, and V-6 (Family B) was unknown.<sup>2</sup> In order to determine whether or not these females were carriers, we had to first establish the molecular genetic cause of BCM in the affected males from each family. An unaffected male from Family A (III-5) and an unrelated male with normal vision (JN) were used as controls in the genetic analyses.

#### 2.2.2. Real-time PCR

Using a previously described quantitative real-time polymerase chain reaction (PCR) assay (Neitz & Neitz, 2001) we estimated the relative ratio of first versus downstream genes in the X-chromosome opsin gene arrays. Quantitative real-time PCR was also used to estimate the relative ratio of L to M genes in each X-chromosome array as previously described (Neitz & Neitz, 2001).

#### 2.2.3. Identifying the deletion and mapping the deletion endpoints in affected males

Primers and PCR conditions are given in Table 1. PCR was used to amplify a 0.16 kb DNA segment spanning the LCR 37 bp core element that is required for transcription of the X-chromosome cone pigment genes using primer pair 1. Deletion of this element is a common cause of BCM (Nathans et al., 1989, 1993). For males in which no PCR product was obtained with primer pair 1, DNA samples were then analyzed using primers pairs 2, 3, and 4, which amplify different segments that lie 7.5, 8.4, and 9.3 kb, respectively, upstream of the first gene in an intact array. For each amplification, if no PCR product was obtained it was assumed that it corresponded to a region that was encompassed by the deletion. These reactions identified the general region of the 5' end of the putative deletion. Primer pairs 5–7 were used to identify the general region of the putative 3' end of the deletion. Primer pairs 6 and 7 were used to amplify a DNA segment that spanned the deletion endpoints for affected members in Families A and B, respectively. The PCR products from primer pairs 6 and 7 were directly sequenced using previously described methods (Neitz et al., 2004), allowing us to identify the exact locations of the deletion endpoints in the affected members of each family.

#### 2.2.4. Determining status of females who were potential carriers of the deletion

Primer pairs 6 and 7 were used to amplify DNA from obligate carrier females and females of unknown carrier status from both families. The PCR conditions were designed to amplify the smaller fragment associated with the deletion rather than the wild type fragment. For the obligate carriers, the small fragment indicating the presence of the deletion was obtained, and served as a positive control. For the females of unknown carrier status, the presence of the smaller fragment indicated the female was a carrier, and the absence of the fragment indicated the female was not a carrier.

#### 2.2.5. Confirmation of non-carrier status

In the females for whom no smaller fragment was identified using primer pair 6 (Family A) or 7 (Family B), direct sequencing was used to confirm non-carrier status. Long distance PCR was used as previously described to selectively amplify the L pigment genes for IV-6 (Family A) and V-4 (Family B). Exons 2, 3 and 4 of the L genes were subsequently amplified and directly sequenced. These results were compared to sequencing data from affected

<sup>2</sup> A few years after participation in this study, V-2 (Family B) had a son (VI-1) who was subsequently diagnosed with BCM, thus classifying her as a carrier. This corroborated our genetic results, which were obtained prior to her son being born.

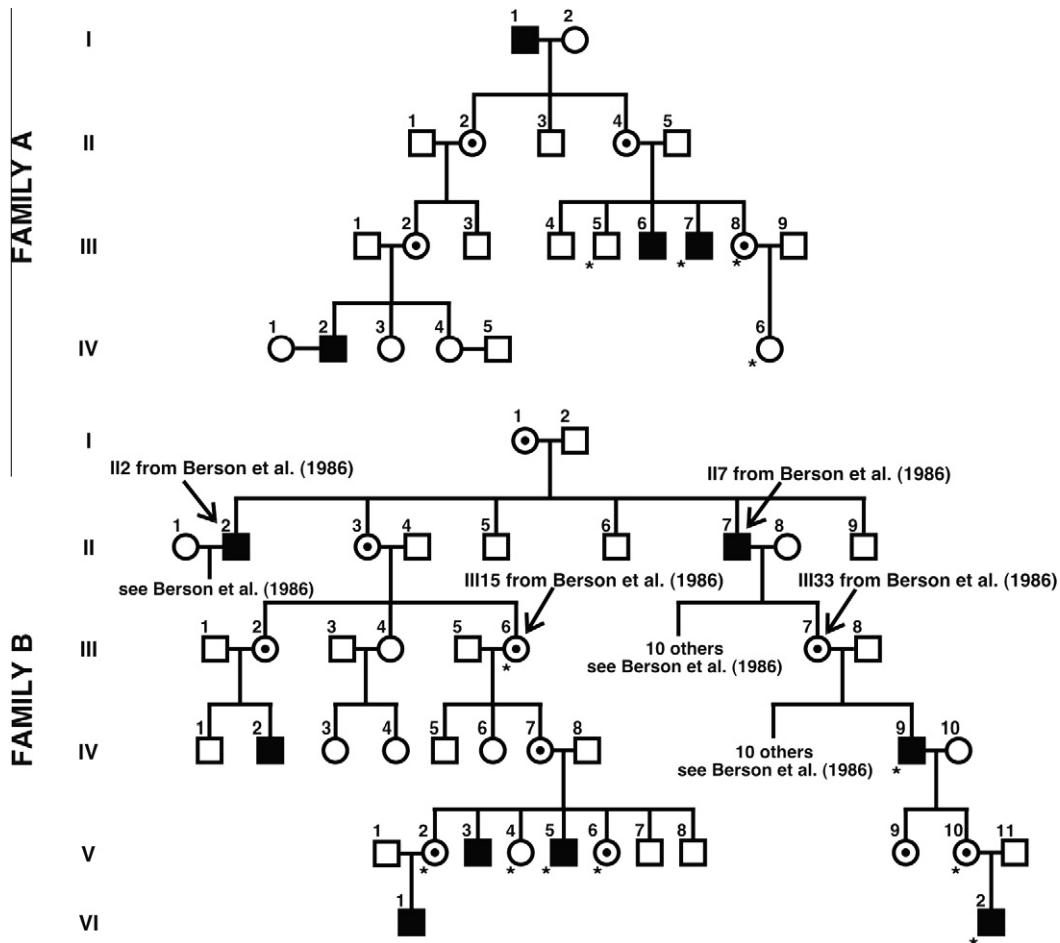


**Fig. 1.** BCM pedigrees showing X-linked recessive inheritance. Filled squares are affected males by history; circles with central dot are female carriers (obligate or genetically determined). Open circles and squares represent unaffected females and males, respectively. Asterisks represent subjects for whom genetic analyses were completed. Adaptive optics images were acquired from subjects III-8 and IV-6 in Family A, and IV-7, V-2, V-4, and V-6 in Family B. Family B was determined to be one of the families reported by Berson et al. (1986); known links between the two pedigrees are indicated.

males or female carriers in order to verify the non-carrier status of IV-6 (Family A) and V-4 (Family B).

2.3. Clinical electroretinography

For five of the six females, full-field, single-flash, and 30 Hz flicker ERG responses were recorded (UTAS-E2000 or E4000 system; LKC Technologies Inc., Gaithersburg, MD) according to published standards (Marmor, Holder, Seeliger, & Yamamoto, 2004). Burian-Allen bipolar electrodes were used as the active corneal and reference electrodes. The ground electrode was placed on the forehead. Rod responses were measured using a dim (2.5 cd/m<sup>2</sup>) flash after 30 min of dark adaptation. Combined rod/cone responses were acquired using maximum intensity flashes (600 cd/m<sup>2</sup>). Photopic cone responses were elicited in light adaptation to a white background (29 cd/m<sup>2</sup>) and with maximum flash stimulation.

2.4. Cone mosaic imaging with adaptive optics (AO)

Each subject's eye was dilated and accommodation paralyzed through use of phenylephrine hydrochloride (2.5%) and tropicamide (1%). Imaging was done using an adaptive optics flood-illuminated fundus camera (Hofer et al., 2001; Pallikaris, Williams, & Hofer, 2003) and/or an adaptive optics scanning laser ophthalmoscope (AOSLO) (Zhang, Poonja, & Roorda, 2006; Zhang & Roorda, 2006).

The AO flood-illuminated system measures the eye's monochromatic aberrations over a 6.8-mm pupil using a Shack-Hartmann wavefront sensor. A 97-channel deformable mirror (Xinetics, Devins, MA) was used for aberration correction. Following wavefront correction, we used a krypton arc flash lamp to illuminate the retina with a 4-ms, ~0.3 μJ flash [650 or 550 nm, 40-nm bandwidth (full width at half max)]. Individual 1-degree diameter images were acquired with a CCD (Roper Scientific, Trenton, NJ). A paper fixation target, placed optically conjugate with the subject's retina, was used to guide the retinal location being imaged along the horizontal meridian.

The AOSLO system also used a Shack-Hartmann wavefront sensor to measure aberrations over a 6-mm pupil. Wavefront correction was achieved using a 144-channel MEMS deformable mirror (Boston Micromachines Corp., Cambridge, MA). A superluminescent diode (Superlum BroadLighter, S840-B-1-20) with a mean wavelength of 840 nm and a spectral full-width-at-half-maximum of 50 nm was used to simultaneously correct the eye's aberrations and image the retina. Retinal images were obtained over a field size of 0.8 × 0.9° using a retinal illuminance of ~2.4 log Trolands (laser power of 160 μW). Several AOSLO videos were acquired, at a frame rate of 30 Hz. The preferred retinal locus of fixation (PRLF) was imaged first and then a fixation target was repositioned such that overlapping retinal areas could be imaged, from the PRLF to about 2.5° temporal. System magnification was calculated as previously described to account for changes imposed by using spectacle

**Table 1**  
Primer pairs used for mapping BCM deletions and determining carrier status.

Pair	Name	Primer sequence	Position	Concentration (nm)	Region amplified	PCR conditions/volume	Enzyme
1	Lcrcode1F	5'GCCCCACAGGTGCTGAGTACT	3.58 kb upstream of mRNA start site	900	LCR core	95 °C 9 min; 94 °C 15 s, 69 °C 1 min, 40 cycles; 72 °C 7 min, 4 °C hold/50 µL	Gold
	Lcrcode1r	5'AGAGTGGAGGTGGCAGAGGTGGGAG	3.42 kb upstream of mRNA start site	900			
2	CpG38Fwd1	5'CGACCAGGATCCACCCCTTTC	7.53 kb upstream of mRNA start site	300	CpG38 marker	94 °C 1 min; 94 °C 15 s, 63 °C 30 s, 72 °C 1 min, 35 cycles; 72 °C 10 min, 4 °C hold/100 µL	xL
	CpG38Rev1	5'GCGGAAGGAGAGACATAATGG	6.94 kb upstream of mRNA start site	300			
3	Up1000CpG38Fwd1	5'TCAAATCATCAGATCCAAGACTCTAAGACA	8.41 kb upstream of mRNA start site	900	1 kb upstream of CpG38 marker	95 °C 9 min; 94 °C 15 s, 66 °C 30 s, 35 cycles; 72 °C 7 min, 4 °C hold/50 µL	Gold
	Up1000CpG38Rev1	5'AAAGCTTCTACTGCCTTTGAACAGAAAAC	8.23 kb upstream of mRNA start site	900			
4	Up2000CpG38Fwd1	5'TAATTACAAAGGATTTGCAGGGAACAAG	9.33 kb upstream of mRNA start site	900	2 kb upstream of CpG38 marker	95 °C 9 min; 94 °C 15 s, 65 °C 30 s, 35 cycles; 72 °C 7 min, 4 °C hold/50 µL	Gold
	Up2000CpG38Rev1	5'AAATGGAGAAATAGAGAAAGGGCAAGAG	9.17 kb upstream of mRNA start site	900			
5	Up1000CpG38Fwd1	5'TCAAATCATCAGATCCAAGACTCTAAGACA	8.41 kb upstream of mRNA start site	900	1 kb upstream of CpG38 marker to exon 6 of adjacent gene, spans BCM deletion	94 °C 3 min; 94 °C 15 s, 66 °C 4 min, 10 cycles; 94 °C 15 s, 66 °C 4 min + 20s/cycle, 18 cycles; 68 °C 10 min, 4 °C hold/100 µL	xL
	E6	5'GCAGTGAAAGCCTCTGTGACT	29 bp downstream of Poly A signal	900			
6	Up1000CpG38Fwd1	5'TCAAATCATCAGATCCAAGACTCTAAGACA	9.33 kb upstream of mRNA start site	900	1 kb upstream of CpG38 marker to exon 2 of adjacent gene, spans BCM deletion	94 °C 3 min; 94 °C 15 s, 66 °C 3 min, 28 cycles; 68 °C 10 min, 4 °C hold/100 µL	xL
	889–862Rev	5'TGTAGCCCTCCAGGACACACATAGGGT	Exon 2	900			
7	Up2000CpG38Fwd2	5'TAATTACAAAGGATTTGCAGGGAACAAG	9.33 kb upstream of mRNA start site	900	2 kb upstream of CpG38 marker to exon 2 of adjacent gene, spans BCM deletion	94 °C 3 min; 94 °C 15 s, 66 °C 3 min, 28 cycles; 68 °C 10 min, 4 °C hold/100 µL	xL
	889–862Rev	5'TGTAGCCCTCCAGGACACACATAGGGT	Exon 3	900			

lenses to correct for each subject's refractive error (Rossi, Weiser, Tarrant, & Roorda, 2007).

### 2.5. Analysis of the cone mosaic

For images acquired with the AO flood-illuminated system, individual frames from the same retinal location were registered with subpixel accuracy (accounting for translation and rotation) and averaged using a custom MatLab (MathWorks, Natick, MA) image registration program (Putnam et al., 2005). Between 3 and 12 individual frames were used to create each of the images used for analysis. Cone density was calculated for each summed image using previously published methods (Carroll et al., 2004) as well as a modified version of a software program that has been used

to automatically identify photoreceptors in AO retinal images (Li & Roorda, 2007).

AOSLO videos were processed as described elsewhere (Rossi & Roorda, 2010). For one subject (Family B, V-2), we applied blind deconvolution to retinal images to better resolve cone centers near the PRLF. A Matlab function (deconvblind) was used as the initial point-spread function (PSF) in the iterative blind deconvolution process; the size of the initial PSF used (initpsf) was 6 pixels. This method was used only when the central-most cones were nearly fully resolved and the signal-to-noise ratio was high in the retinal image. To ensure that we did not falsely identify cones based on amplified noise or other artifacts, deconvolved images were carefully compared to non-deconvolved images and only used to guide the localization of cone centers when they were revealed as being

within a contiguously-packed array. A large montage was subsequently created by overlapping adjacent registered retinal images.

Cone positions were localized on the AOSLO retinal montages using a combination of automated (Li & Roorda, 2007) and manual methods. To determine the neighbors for each cone, cone positions were triangulated using the Delaunay triangulation implementation in Matlab. The distance from each cone to all of its neighbors was calculated geometrically and averaged, resulting in a measurement of inter-cone distance for each cone (Rossi & Roorda, 2010). Cone density was calculated directly by counting cone centers falling in predetermined bounding windows. To ease comparison with other published reports (Curcio, Sloan, Kalina, & Hendrickson, 1990; Curcio, Sloan, Packer, Hendrickson, & Kalina, 1987), a 36.5 μm × 36.5 μm bounding window (~1332 μm<sup>2</sup>) was used. Mosaic regularity was assessed using a larger, 85 μm × 85 μm bounding window for comparison to a previous study of normal observers (Rossi & Roorda, 2010).

### 3. Results

#### 3.1. Quantitative real-time PCR

Table 2 shows the relative ratios of first to downstream genes and of L to M genes, estimated using quantitative real-time PCR. An estimate of 75% downstream genes was interpreted as an array with four genes, one in the first position followed by three additional genes. An estimate of 66% downstream genes was interpreted as an array with three genes (two of them being downstream of the first gene), and an estimate of 50% downstream genes is interpreted as an array with two genes, one in the first position and one downstream of the first gene. An estimate of 100% downstream genes was interpreted as a mutation that is either a deletion involving the first gene in the array, or a point mutation that affects the quantitation. The results of this assay suggest that all of the affected males we analyzed (Family A, III-7 and Family B, V-5, IV-9, and VI-2) had a deletion that affects the X-chromosome cone opsin genes. Subject III-7 in Family A was estimated to lack L genes (0%L), consistent with a deletion that includes the entire L gene. The estimates of the %L genes in the L/M array for the af-

ected males in Family B were consistent with them having intact L genes. This is consistent with previous findings that L/M arrays can contain multiple L genes, even in individuals with normal color vision (Sjoberg, Neitz, Balding, & Neitz, 1998).

#### 3.2. Deletion-mapping results

The inferred extent of the L/M array deletion for each family is shown in Fig. 2. Using PCR primer pair 1 to amplify the core element of the LCR failed to yield a product for the affected males in both families (Family A, III-7; Family B, V-5, IV-9, and VI-2), but both positive controls (unaffected male III-5, Family A and JN) did yield the expected fragment. This is consistent with the affected males having an L/M array containing a deletion that encompasses the LCR. As described above, the endpoints of the putative deletions were localized using PCR with primers pairs 2, 3, 4 and 5, and either primer pair 6 (Family A) or 7 (Family B). The PCR products from primer pairs 6 and 7 were directly sequenced to determine the precise endpoints of the deletion.

For the affected male in Family A (III-7), primer pair 2 did not yield a PCR product, but primer pair 3 did; localizing one deletion endpoint to a region of the chromosome between these PCR targets. Amplification of DNA with primer pair 5 yielded a 9 kb fragment, which is smaller than the expected 23 kb product. Primer pair 6 yielded a 0.45 kb PCR product rather than a 15 kb product expected from an intact array. The 0.45 kb product was directly sequenced and revealed a deletion of nucleotides 153,054,920–153,106,698 (USCS Genome Database, February 2009 build).

For the affected males in Family B (V-5, IV-9, and VI-2), primer pairs 2 and 3 did not yield a PCR product. Primer pair 4 yielded a PCR product that was slightly larger than the corresponding fragment from Family A (Table 2), and direct sequencing revealed a 26 bp insertion. The sequence of the 26 bp insert is: 5'AGA CAATAGTCTAATAGTCATAACAAT, and a blast search of the human genome does not reveal any matches to this sequence. The affected members of this family also yielded a PCR product that was smaller than expected from an intact array with primer pair 7 (Table 2). Direct sequencing of the 0.55 kb PCR product obtained with primer pair 7 revealed a deletion of nucleotides 153,053,783–153,069,342.

**Table 2**  
Summary of genetic results.

Subject	Status	%L <sup>a</sup>	%DS <sup>a</sup>	Primer pair <sup>b</sup>						
				1 <sup>c</sup>	2 <sup>c</sup>	3 <sup>c</sup>	4 <sup>d</sup>	5 <sup>e</sup>	6 <sup>f</sup>	7 <sup>g</sup>
Family A, III-5	Male, unaffected	43	72	+	+	+	nd	nd	–	nd
Family A, III-7	Male, affected	0	100	–	–	+	nd	+	+	nd
Family A, III-8	Female, carrier	23	73	nd	nd	nd	nd	+	+	nd
Family A, IV-6	Female, non-carrier	65	37	nd	nd	nd	nd	nd	–	nd
Family B, III-6	Female, obligate carrier	49	83	nd	nd	nd	*	nd	nd	+
Family B, V-2	Female, carrier	60	76	nd	nd	nd	*	nd	nd	+
Family B, V-5	Male, affected	66	100	–	–	–	+	nd	nd	+
Family B, V-6	Female, carrier	46	79	nd	nd	nd	*	nd	nd	+
Family B, IV-9	Male, affected	64	100	–	–	–	+	nd	nd	+
Family B, V-10	Female, obligate carrier	61	71	nd	nd	nd	*	nd	nd	+
Family B, VI-2	Male, affected	64	100	–	–	–	+	nd	nd	+
Family B, V-4	Female, non-carrier	nd	nd	nd	nd	nd	–	nd	nd	–
JN	Male, normal control	52	57	+	+	+	–	nd	nd	–

<sup>a</sup> Quantitative real-time PCR was used to estimate the percentage of downstream genes and the percentage of L genes in each X-chromosome array as previously described (Neitz & Neitz, 2001).

<sup>b</sup> Primer Pairs given in Table 1. Expected sizes for an intact array are 0.159 kb (pair 1), 0.546 kb (pair 2), 0.182 kb (pair 3), 0.162 kb (pair 4), 23 kb (pair 5), 15 kb (pair 6), 16 kb (pair 7), and “nd” = not done.

<sup>c</sup> “+” = PCR product of expected size was obtained and “–” = no PCR product obtained.

<sup>d</sup> “+” = Presence of 26 bp larger than expected fragment, “–” = normal sized PCR product obtained, and “\*” = both larger and normal fragments obtained.

<sup>e</sup> “+” = Smaller PCR fragment obtained (9 kb).

<sup>f</sup> “+” = Smaller PCR fragment obtained (0.45 kb) and “–” = absence of smaller PCR fragment.

<sup>g</sup> “+” = Smaller PCR fragment obtained (0.55 kb) and “–” = absence of smaller PCR fragment.

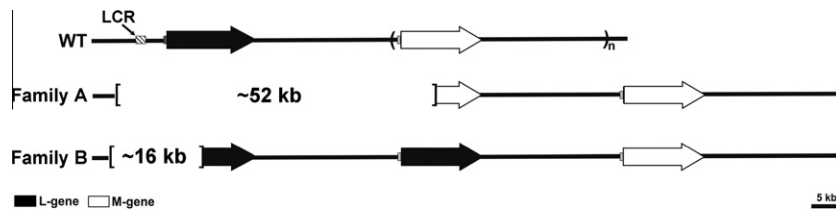


**Fig. 2.** Diagram of BCM genotypes found in this study. Each arrow represents an L or M gene. The L and M genes reside in a head-to-tail tandem array, which is variable in gene number. The most common configuration among individuals with normal color vision is to have 1 L gene (filled arrows) followed by 1 or more M genes (open arrows). Each L or M gene is preceded by a proximal promoter (shaded gray boxes) and the entire array has a single locus control region (LCR) that is essential for the expression of genes from the array (hatched box). The deletion in Family A was about 52 kb in length, and included the LCR, the entire first gene in the array, and part of the second gene in the array. The deletion in Family B was about 16 kb in length, and included the LCR and part of the first gene in the array.

### 3.3. Determination of carrier status – Family A

The carrier status of females III-8 and IV-6 in Family A was evaluated using primer pair 6 to amplify the deletion endpoints. A PCR product was obtained from III-8 but not for IV-6, consistent with III-8 being a carrier and IV-6 not being a carrier. Since the results of real-time PCR indicated that the X-chromosome associated with BCM in Family A lacked intact L genes, we directly amplified the L genes from III-8 and IV-6 and directly sequenced exons 2, 3 and 4. Subject IV-6 had more than one L-opsin gene sequence, which is consistent with having intact L genes on both X-chromosomes, and hence not being a carrier of BCM. Thus, we concluded that III-8 was a carrier of BCM and we identified a PCR product that spans the deletion endpoints in a similar fashion as described for the affected male in Family A (III-7).

### 3.4. Determination of carrier status – Family B

For Family B, both obligate carriers (III-6 and V-10) gave both the normal and the 26 bp larger PCR products with primer pair 4 and gave the small PCR product with primer pair 7 confirming her carrier status. A PCR product was obtained from females V-6 and V-2 with primer pair 7 indicating that both are carriers of BCM. Both the large and normal sized PCR products were obtained with primer pair 4 from these females, also consistent with their carrier status. A product was not obtained with primer pair 7 for V-4. In addition, this female had the normal size PCR product with primer pair 4 consistent with her not being a carrier.

Further confirmation of status of V-4 as a non-carrier of the X-chromosome with the LCR deletion comes from the fact that the intact L-opsin gene on the X-chromosome in Family B specifies the following amino acids at the polymorphic positions in exons 2, 3, and 4: isoleucine 65, valine 111, tyrosine 116, leucine 153, valine 171, alanine 174, isoleucine 178, alanine 180, threonine 230, serine 233, valine 236, abbreviated “IVY LVAIA TSV” using the single letter amino acid code. Female carriers V-2 and V-6 had this opsin gene, whereas V-4 had two L-opsin sequences, “TIS LVAIA IAM” and “TIS LVAIS IAM” (M is the single letter amino acid code for methionine). Thus, neither of V-4’s L-opsin genes matched the one found on the X-chromosome containing the LCR deletion, thereby providing further evidence that she does not carry the BCM-causing X-chromosome. While none of the opsin genes on the X-chromosome with the LCR deletion are expressed, the L-opsin gene sequence provides additional information with which to distinguish between carriers and non-carriers in this family.

### 3.5. Decreased cone density in BCM carriers

Cones were resolved at or near the foveal center for all carrier eyes. This observation alone indicates increased cone spacing relative to normal observers, as it is typically not possible to resolve the smallest foveal cones in normal eyes using adaptive optics imag-

ing. Retinal image quality varied considerably between subjects and between imaging systems. Cone contrast was generally superior in the AOLSO images, due to the confocal nature of the system which rejects light scattered from non-photoreceptor layers. Fig. 3 shows retinal images at  $\sim 1^\circ$  from fixation in the six females from the BCM families, and a single normal control. Qualitative differences in the density and regularity of the mosaics are evident between the carriers and the non-carriers. On average, the four carriers had reduced density compared to normal while the two non-carrier females had normal cone densities (Fig. 4a). There was some difficulty in identifying every cone at the PRLF in all of the images, with cones being most difficult to resolve in carrier V-2 (Family B), who had the highest cone density of the carriers examined. Deconvolution helped to resolve cone centers near the PRLF for this subject (see Section 2.5). Peak foveal cone density was directly measured in both eyes of subject IV-7 (Family B) and one eye each from V-2 (Family B) and III-8 (Family A). For these BCM carriers, foveal cone density ranged from 75,936 to 106,010 cones/mm<sup>2</sup>, with a mean of 94,921 cones/mm<sup>2</sup>. Interestingly, the location of peak density in these carriers was displaced from the measured PRLF by about 6  $\mu$ m on average. A similar displacement, though of a larger magnitude, has been previously reported for normal observers (Putnam et al., 2005). While these values may slightly underestimate the actual peak foveal cone density (due to the inability to resolve every single cone at the fovea), it is apparent that compared to published normative values from histology (Curcio et al., 1990), the BCM carriers have reduced peak foveal cone density (Fig. 4b). Central foveal cone density was not measured in the AO flood-illuminated images, as the location of the PRLF was not obtained.

### 3.6. Electroretinogram (ERG) results

A well-described phenotype associated with carriers of BCM is abnormal cone ERG’s (Berson et al., 1986; Spivey et al., 1964). In the largest study present in the literature, Berson et al. (1986) remarked that all seven obligate carriers from two families with BCM showed some ERG abnormalities, with 6 out of 7 showing delayed cone b-wave implicit times to 30-Hz flicker. They also observed that the obligate carriers had average cone amplitudes that were about 50% of normal. Fig. 5 shows results from the three carriers from whom we were able to obtain ERG recordings. There was variability across the three carriers, with some showing significantly reduced cone ERG amplitudes (e.g., Family A, III-8) and others having near normal amplitudes (e.g., Family B, V-6). Interestingly, these same two carriers also had a slight delay in 30-Hz implicit time. This variable ERG phenotype is generally consistent with that observed by Berson et al. (1986). As we only have ERG data on three carriers, it is difficult to draw any correlations between the appearance of the cone mosaic and the ERG phenotype. However subject III-8 (Family A) was shown to have the lowest cone density of all the carriers (Fig. 4), and she also manifested the greatest ERG abnormality. In addition, our Family B reported here (in whom we have shown a sig-

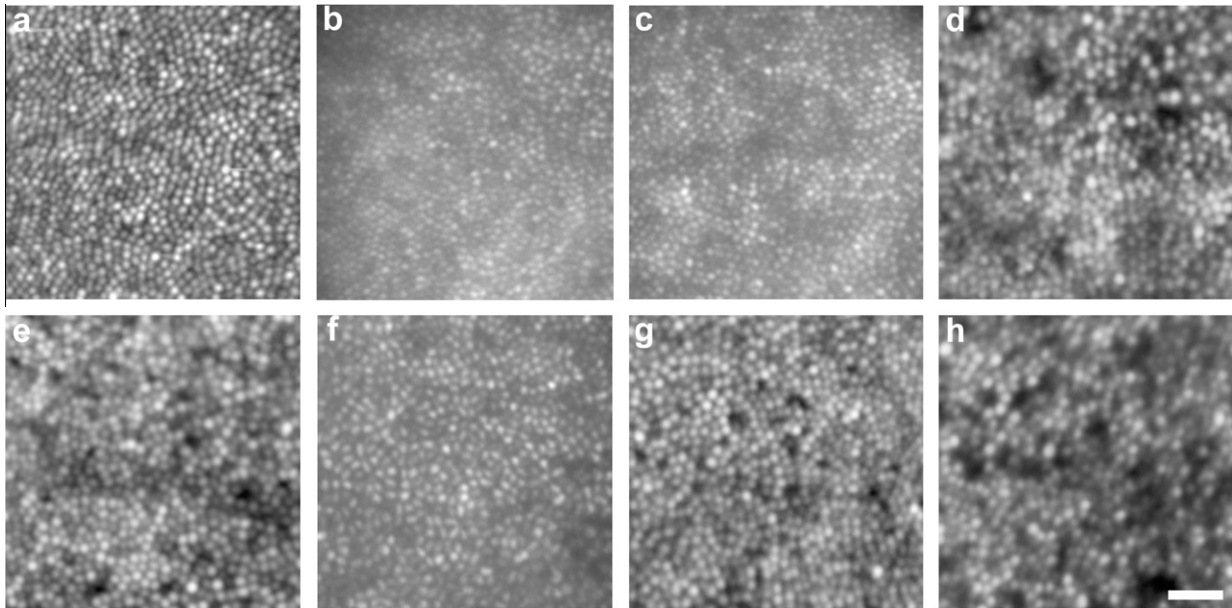


**Fig. 3.** Appearance of the cone mosaic in carriers of BCM. Each image is  $0.5^\circ \times 0.5^\circ$ , centered approximately  $1^\circ$  from the center of fixation. (a) Normal trichromat control, (b) non-carrier (Family A, IV-6), (c) non-carrier (Family B, V-4), (d) BCM carrier (Family A, III-8), (e) BCM carrier (Family B, V-2), (f) BCM carrier (Family B, V-6), (g) BCM carrier (Family B, IV-7, left eye), and (h) BCM carrier (Family B, IV-7, right eye). Scale bar is 0.5 arc min.

nificant reduction in cone density) is one of the two families originally reported by Berson et al. (1986), in whom the ERG phenotype was thoroughly documented. Thus, we conclude that the presence of an ERG phenotype in carriers of BCM is due to a reduced number of cone photoreceptors, rather than reduced function or reduced optical density of a normal number of cones.

### 3.7. Regularity of the cone mosaic

For the three BCM carriers imaged on the AOSLO, mosaic regularity was assessed relative to the PRLF. Voronoi analysis was performed as previously described (Baraas et al., 2007; Li & Roorda, 2007; Rossi & Roorda, 2010). The Delaunay triangulation that was used to compute inter-cone distance was used to evaluate the number of neighbors of each cone. In a perfectly regular triangular lattice arrangement each cone has six neighbors. However, a perfect triangular lattice arrangement is not found in the human retina (Curcio & Sloan, 1992; Pum, Ahnelt, & Grasl, 1990), because a regular packing arrangement cannot be maintained when the spacing between receptors is rapidly changing, as it does in the macular region. Shown in Fig. 6a is a Voronoi diagram of the cone mosaic for a representative normal eye previously reported by Rossi and Roorda (2010). The Voronoi diagrams for the three BCM carriers are shown in Fig. 6b–d. As can be appreciated from visual inspection of the diagrams, even the normal mosaic is far from perfectly regular. However, the mosaics from the BCM carrier retinas were even further disrupted. Shown in Fig. 6e is a plot of the percentage of cones having six neighbors, averaged at  $0.1^\circ$  intervals for the three carriers (open circles). For comparison, the average of six normal eyes is also shown (filled circles). The maximum percentage of cones with six neighbors for normal eyes ranged from 54.6% to 75.5% at locations between  $0.56^\circ$  and  $1.75^\circ$  from the PRLF. The average maximum percentage of cones with six neighbors was 66.1% for the normal eyes ( $SD = 7.7\%$ ). The maximum percentage of cones having six neighbors was 56.9%, 55.6%, 57.3% and 58% for subject IV-7, OS (Family B), IV-7, OD (Family B), subject V-2 (Family B) and subject III-8 (Family A), respectively. Interestingly, the location at which this maximum occurred was variable across the retinas. The peak regularity occurred at eccentricities of  $0.95^\circ$ ,  $0.59^\circ$ ,

$1.1^\circ$ , and  $2.69^\circ$  for subject IV-7, OS (Family B), IV-7, OD (Family B), subject V-2 (Family B) and subject III-8 (Family A), respectively. The mosaics in the BCM carriers are noticeably disrupted around  $1^\circ$  from the PRLF (Fig. 6e), as they lack the typical peak in regularity observed in most normals. This is likely due to the constraints of tight packing being reduced in the carrier due to them having fewer cones. Further conclusions will have to await a systematic comparison of mosaic regularity as a function of cone density, rather than a function of retinal eccentricity.

### 3.8. Appearance of the cone mosaic – AO flood-illuminated versus AOSLO

We acquired retinal images in one female carrier (V-2 from Family B), using both the AOSLO and AO flood-illuminated systems. While density estimates were in good agreement, we observed interesting differences when comparing the appearance of individual cones at the same retinal location. Shown in Fig. 7 are images from  $0.5^\circ$  (Fig. 7a–c) and  $1^\circ$  temporal to the fovea (Fig. 7d–f). At both locations, more than 97% of the cones were visible with both imaging systems, despite the fact that the images were taken nearly two years apart. However, there were some discrepancies, even after correcting for edge artifacts caused by the two images not being 100% coincident, and using our best efforts to align them. In the  $0.5^\circ$  image, there were 16 cones that appeared only in the AO flood-illuminated image and 3 cones that appeared only in the AOSLO image; a net difference of 13 cones, reflecting a difference of less than 2% of the 810 cones in the AO flood-illuminated image. In the  $1^\circ$  image, there were 59 cones that appeared only in the AO flood-illuminated image and 27 cones that appeared only in the AOSLO image; a net difference of 32 cones, reflecting a difference of less than 3% from the 1108 cones in the AO flood-illuminated image.

## 4. Discussion

### 4.1. Determining carrier status in potential BCM carriers

The genetic approach outlined here offers an efficient method for determining carrier status in instances where the condition is

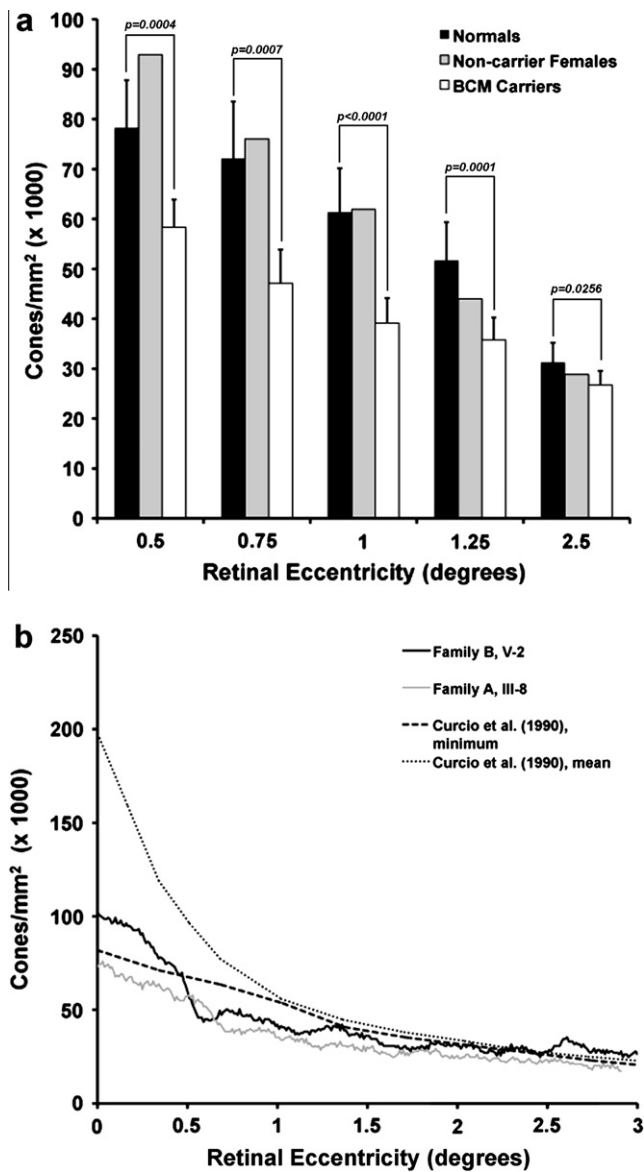


**Fig. 4.** Cone density as a function of retinal eccentricity. (a) Cone density was averaged for between eight and 14 normals (dark filled bars) and all four BCM carriers (open bars). Error bars indicate + 1 SD. Cone density for the two non-carrier females (Family A, IV-6 and Family B, V-4) is also shown (gray bars). (b) Cone density along the temporal meridian for the BCM carriers with the minimum (Family A, III-8) and maximum (Family B, V-2) foveal cone density. Plotted for comparison is the minimum and mean normal cone density from Curcio et al. (1990).

caused by a deletion of the LCR – however, it is important to have access to affected and unaffected males from within the family to help with diagnosis. In families where the presence of a missense mutation is in a single-gene array (“two-step” mutational pathway), determination of carrier status would be more straightforward, though again access to affected and unaffected males within the family is helpful. Given the variability in the ERG phenotype shown previously (Berson et al., 1986) and in this study, molecular genetic evaluation is far more reliable for definitively establishing carrier status. For many females from families with a history of BCM, knowing their carrier status is important for genetic counseling, especially as they consider having children.

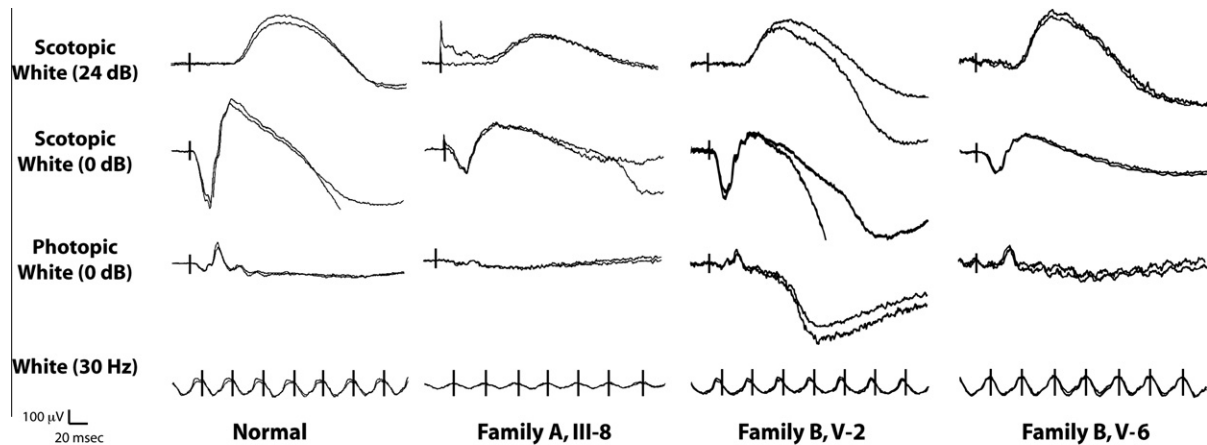
All of the females that were shown to be carriers had disrupted cone mosaics, though to a variable degree. Thus, imaging of the cone mosaic could play a diagnostic role in determining carrier

status, especially in cases where genetic analysis is unavailable or inconclusive. However, given the wide range of “normal” X-inactivation levels (Sharp, Robinson, & Jacobs, 2000), one would want to use caution in using a negative imaging result to infer non-carrier status. For example, a female carrier of BCM could have a skewed ratio of inactivation of the X-chromosome containing the BCM-conferring L/M array. Such a carrier may not present a phenotype, even at the level of the cone mosaic – though assessment of mosaic regularity has been shown to detect significant disruption when only about 5% of the cones have been compromised (Baraas et al., 2007). It may be that no such carrier practically exists for whom the mosaic would not be disrupted to some detectable degree. However, until we directly examine such retinas, molecular diagnosis remains the only way to confirm carrier status.

#### 4.2. Appearance of the cone mosaic – AO flood-illuminated versus AOSLO

There are a number of potential sources for our observed discrepancy between the images obtained from the two systems. First, it could be that there were real changes in the cone mosaic over the 2-year period. Certainly the fact that, on average, more cones were seen in the flood-illuminated AO image than the AOSLO image (which was the most recently acquired image) would be consistent with this hypothesis. However, that we observed some cones in the more recent AOSLO images that were not originally seen in the flood-illuminated AO images argues against this idea. A second possibility is that these differences are due to differences in the light source used in each AO system. The AOSLO uses a partially coherent source whereas the flood-illuminated AO system employs an incoherent source. Since it is believed that the reflectance from a given cone originates from multiple surfaces (Pallikaris et al., 2003; Rha et al., 2006), a coherent source could cause these signals to constructively and destructively interfere, causing the cone to become brighter and dimmer, respectively. Even with a partially coherent source, it is possible that small amounts of interference arise from multiple reflections within a cone, between neighboring cones, or even from adjacent rods. This predicts that the variability in cone reflectance will be greater in AOSLO images versus flood-illuminated AO images, though more data is required to sufficiently test this hypothesis. A third possibility is that the 8-bit detection system employed by the AOSLO may not have enough dynamic range to detect the few dimmest cones.

These differences in cone identity will induce small errors in spacing and regularity measurements. Depending on the methods used to evaluate density and spacing, it could have the following effects for the AOSLO images: increased cone spacing, reduced cone density, and decreased mosaic regularity. Cone spacing increases would only be seen if cone spacing was measured directly, because of the small number of missing cones and their sporadic appearance within the image, measurement techniques such as the density recovery profile most likely would not reveal increased spacing (Rodieck, 1991). Cone density estimates based on direct counting of the cones results in measurements of 43,417 cones/mm<sup>2</sup> and 44,686 cones/mm<sup>2</sup> for the AOSLO and AO flood-illuminated images, respectively (a difference of less than 3%). These measurement errors appear to be smaller than those that arise due to different humans manually localizing cones in AOSLO images (Li & Roorda, 2007). Nevertheless, no matter the origin of the observed differences, or the magnitude of their impact on the spatial analysis, it is important to keep in mind that the absence of a reflected cone signal cannot always be interpreted as an absence of a cone. We believe this is what is happening here; the cones are most likely present but were not reflective enough to be seen in the AOSLO image at the time of imaging.



	Scotopic 24 dB μV	Scotopic 0 dB μV	Photopic 0dB μV	30 Hz Amplitude μV	30 Hz Implicit Time ms
Family A, III-8*	180	349	30	42	32
Family A, IV-6	335	605	148	87	29
Family B, V-2*	249	482	122	97	29
Family B, V-6*	346	627	152	111	31
Family B, V-4	329	646	150	107	29
<b>Normal</b>	<b>&gt;185</b>	<b>&gt;419</b>	<b>&gt;102</b>	<b>&gt;70</b>	<b>&lt;30</b>

\*Carrier

**Fig. 5.** Reduced cone function in BCM Carriers. Shown are electroretinograms from three of the BCM carriers and a normal control. Both rod and cone responses appear reduced in the carriers compared to the non-carriers, though this is variable. Normal values are specific to the instrument used to collect the clinical ERG data, and there is substantial normal variation.

4.3. Variable cone mosaic phenotypes offer insight into timing/severity of cone loss

The cone mosaics of the BCM carriers examined here were significantly disrupted. The BCM carrier mosaics appeared quite different from those of males with red–green color vision defects caused by pigments with the C203R missense mutation (Carroll et al., 2009; Torti et al., 2009) or deleterious polymorphic sequences (“LIAVA”) within exon 3 (Carroll et al., 2004; Rha et al., 2010). An emerging model based on these various cone mosaic phenotypes and their associated genetic origin is that both the timing and degree of cone photoreceptor degeneration imparted by the different cone opsin genotypes is variable. During development, cones differentiate morphologically at 11–12 weeks of gestation, they become synaptically connected to bipolar cells at around 13 weeks of gestation, and they begin to express cone opsin between 15 and 20 weeks of gestation (Georges, Madigan, & Provis, 1999; Linberg & Fisher, 1990). The human fovea first becomes histologically discernable at about 24 weeks of gestation, and migration and packing of cones to form the mature retina with adult cone densities continues postnatally over the course of years (Provis, Diaz, & Dreher, 1998). Thus, until about 15 weeks of gestation, cone photoreceptor development should proceed normally for patients harboring an LCR deletion as well as for patients harboring genes encoding mutant opsins. At 15 weeks, cones with an active X-chromosome that lacks the LCR are unable to express any L/M opsin gene and may degenerate. In contrast, cones that express a mutant opsin gene (such as LIAVA) may remain viable throughout foveal development. In comparing the mosaic associated with the LIAVA polymorphism to that observed here in the LCR deletion, a reasonable hypothesis is that the cones expressing the LIAVA pig-

ment remain as place holders in the mosaic but lack waveguiding outer segments, whereas the cones in the BCM carrier retina that do not express any L or M opsin due to the presence of the LCR deletion do degenerate completely. We propose that in the BCM carriers who have an LCR deletion on one X-chromosome, the later stages of foveal development (specifically cone photoreceptor migration towards the foveal center) “rescue” the appearance of the cone mosaic<sup>3</sup>. While the remaining cones appear to pack nearly completely, the reduced density and reduced regularity of the residual mosaic can be thought of as signatures of this earlier cone loss. Finally, the normal appearance of the remaining cones is consistent with our hypothesis that the cones without opsin degenerated early in development and they do not affect the viability of neighboring cones expressing normal photopigment. Recently, Lewis, Williams, Lawrence, Wong, and Brockerhoff (2010) showed that in zebrafish, wild type cones persist despite neighboring mutant cone degeneration (i.e., what happens in a cone, stays in a cone). This is in stark contrast to rods, where expression of mutant rhodopsin not only compromises the viability of the rod photoreceptor but also neighboring cones. However, there are cases where males with BCM show progressive, widespread retinal degeneration (Ayyagari, Kakuk, Coats, et al., 1999; Ayyagari, Kakuk, Toda, et al., 1999; Kellner et al., 2004; Michaelides et al., 2005; Nathans et al., 1989), so our understanding of this condition is incomplete.

<sup>3</sup> Such a model precludes using the residual cone density to infer anything about the absolute amount of cone loss. In addition, the normal variation in cone density makes it impossible to interpret the observed reduction in cone density in terms of absolute reduction in cone number.

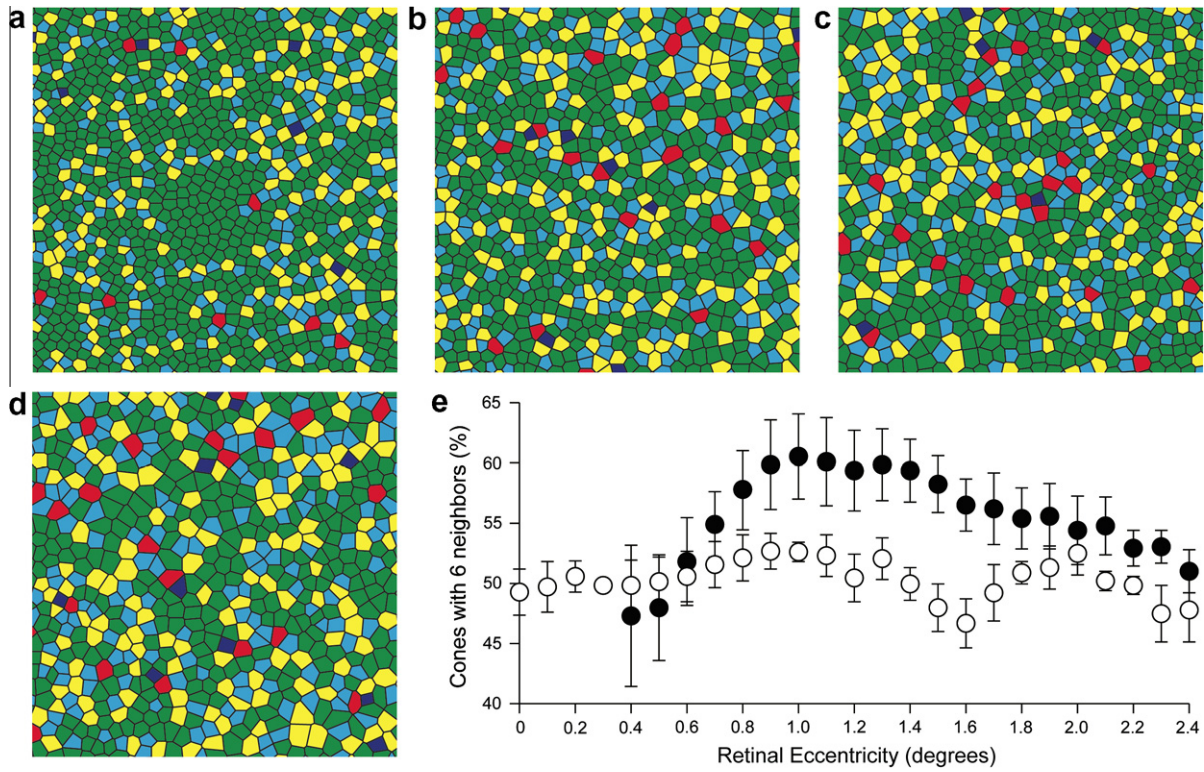


**Fig. 6.** Disrupted regularity of the cone mosaic in the BCM carrier retina. Voronoi diagrams for a normal control (a) and BCM carriers Family B, IV-7 (b), Family B, V-2 (c), and Family A, III-8 (d). Voronoi patch color corresponds to the number of neighbors of each cone, where blue, cyan, green, yellow, and red polygons correspond to cones having,  $\leq 4$ , 5, 6, 7, or  $\geq 8$  neighbors, respectively. (e) Mean percentage of cones having six neighbors, averaged at  $0.1^\circ$  intervals, for the BCM carriers (*open symbols*) and six normal controls (*filled symbols*). Measurements for normal eyes within  $0.3^\circ$  from the PRLF are excluded due to the lack of sufficient data from normal subjects in that area. For the normal eyes, data from five eyes is averaged at the  $0.4^\circ$  location while six eyes are averaged elsewhere. For the BCM carrier eyes, four eyes are averaged between  $0^\circ$  and  $1.4^\circ$  and three eyes elsewhere.

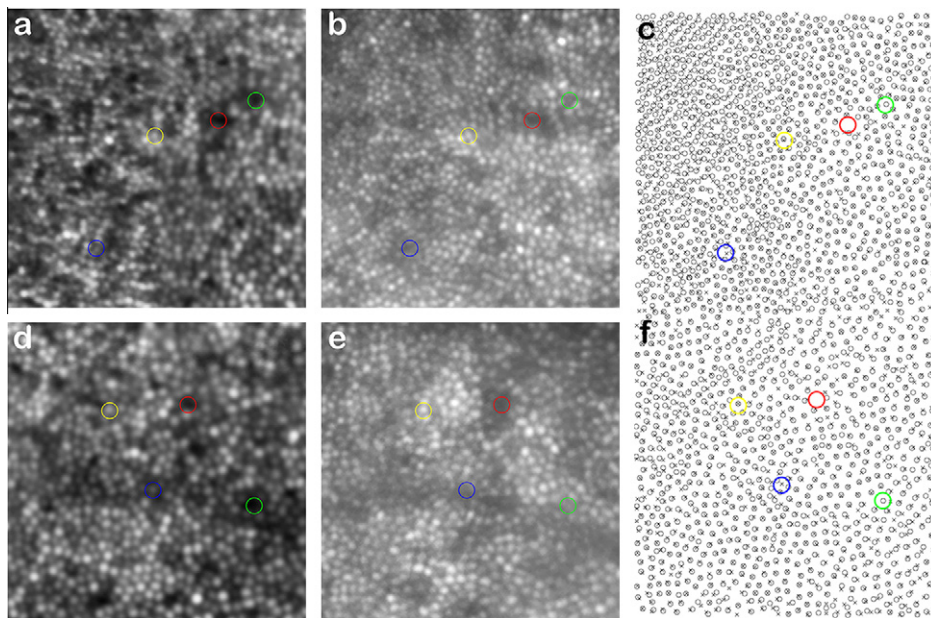


**Fig. 7.** Comparison of retinal images from different AO imaging systems. Shown is a comparison of the same patch of retina from subject V-2 (Family B) imaged nearly 2 years apart on the AOSLO (a, d) and the AO flood-illuminated camera (b, e). (c, f) Cone coordinates obtained from an automated cone identification algorithm, where crosses are cone centers from the AOSLO image, and open circles are cone centers from the AO flood-illuminated system. Red circles indicate positions where no cone was visible in either image, yellow circles indicate positions where a cone was visible in both images, blue circles indicate positions where a cone was visible on the AOSLO image, but not the AO flood-illuminated image, and green circles indicate positions where a cone was visible on the AO flood-illuminated image, but not the AOSLO image. Images a and b are from about  $0.5^\circ$  temporal from fixation, while d & e are from about  $1.0^\circ$  temporal from fixation.

## Acknowledgments

We thank L. Chen, M. Chung, J.L. Duncan, W. Fischer, K. Li, N. Putnam, P. Tiruveedhula, M. Wagner-Schuman, and Y. Zhang for their assistance. We acknowledge financial support from the National Eye Institute (F32-EY014749 & R01-EY017607 to J.C., R01-EY004367 & R01-EY014375 to D.R.W., R01-EY009620 to J.N., R01-EY009303 to M.N., and Core Grants P30-EY001319 & P30-EY001931), and unrestricted departmental grants from Research to Prevent Blindness (Medical College of Wisconsin & University of Rochester). J.C. is the recipient of a Career Development Award from Research to Prevent Blindness. This work has been supported in part by the National Science Foundation Science and Technology Center for Adaptive Optics, managed by the University of California at Santa Cruz under co-operative agreement No. AST-9876783.

## References

- Ayyagari, R., Kakuk, L. E., Bingham, E. L., Szczesny, J. J., Kemp, J. A., Toda, Y., et al. (2000). Spectrum of color gene deletions and phenotype in patients with blue cone monochromacy. *Human Genetics*, *107*, 75–82.
- Ayyagari, R., Kakuk, L. E., Coats, C. L., Bingham, E. L., Toda, Y., Feliuss, J., et al. (1999). Bilateral macular atrophy in blue cone monochromacy (BCM) with loss of the locus control region (LCR) and part of the red pigment gene. *Molecular Vision*, *5*, 13–18.
- Ayyagari, R., Kakuk, L. E., Toda, Y., Coats, C. L., Bingham, E. L., Szczesny, J. J., et al. (1999). Blue cone monochromacy: Macular degeneration in individuals with cone specific gene loss. In J. G. Hollyfield, R. E. Anderson, & M. M. LaVail (Eds.), *Retinal degenerative diseases and experimental therapy*. New York: Kluwer Academic/Plenum Publishers.
- Baraas, R. C., Carroll, J., Gunther, K. L., Chung, M., Williams, D. R., Foster, D. H., et al. (2007). Adaptive optics retinal imaging reveals S-cone dystrophy in tritan color-vision deficiency. *Journal of the Optical Society of America A*, *24*(5), 1438–1446.
- Berson, E. L., Sandberg, M. A., Maguire, A., Bromley, W. C., & Roderick, T. H. (1986). Electroretinograms in carriers of blue cone monochromatism. *American Journal of Ophthalmology*, *102*(2), 254–261.
- Carroll, J., Baraas, R. C., Wagner-Schuman, M., Rha, J., Siebe, C. A., Sloan, C., et al. (2009). Cone photoreceptor mosaic disruption associated with Cys203Arg mutation in the M-cone opsin. *Proceedings of the National Academy of Sciences USA*, *106*(49), 20948–20953.
- Carroll, J., Neitz, M., Hofer, H., Neitz, J., & Williams, D. R. (2004). Functional photoreceptor loss revealed with adaptive optics: An alternate cause for color blindness. *Proceedings of the National Academy of Sciences USA*, *101*(22), 8461–8466.
- Curcio, C. A., & Sloan, K. R. (1992). Packing geometry of human cone photoreceptors: Variation with eccentricity and evidence for local anisotropy. *Visual Neuroscience*, *9*, 169–180.
- Curcio, C. A., Sloan, K. R., Kalina, R. E., & Hendrickson, A. E. (1990). Human photoreceptor topography. *The Journal of Comparative Neurology*, *292*, 497–523.
- Curcio, C. A., Sloan, K. R., Jr., Packer, O., Hendrickson, A. E., & Kalina, R. E. (1987). Distribution of cones in human and monkey retina: Individual variability and radial symmetry. *Science*, *236*, 579–582.
- Gardner, J. C., Michaelides, M., Holder, G. E., Kanuga, N., Webb, T. R., Mollon, J. D., et al. (2009). Blue cone monochromacy: Causative mutations and associated phenotypes. *Molecular Vision*, *15*, 876–884.
- Georges, P., Madigan, M. C., & Provis, J. M. (1999). Apoptosis during development of the human retina: Relationship to foveal development and retinal synaptogenesis. *Journal of Comparative Neurology*, *413*(2), 199–208.
- Gottlob, I. (1994). Eye movement abnormalities in carriers of blue-cone monochromatism. *Investigative Ophthalmology and Visual Science*, *35*, 3556–3560.
- Gross, A. K., Decker, G., Chan, F., Sandoval, I. M., Wilson, J. H., & Wensel, T. G. (2006). Defective development of photoreceptor membranes in a mouse model of recessive retinal degeneration. *Vision Research*, *46*, 4510–4518.
- Hofer, H., Chen, L., Yoon, G. Y., Singer, B., Yamauchi, Y., & Williams, D. R. (2001). Improvement in retinal image quality with dynamic correction of the eye's aberrations. *Optics Express*, *8*(11), 631–643.
- Humphries, M. M., Rancourt, D., Farrar, G. J., Kenna, P., Hazel, M., Bush, R. A., et al. (1997). Retinopathy induced in mice by targeted disruption of the rhodopsin gene. *Nature Genetics*, *15*(2), 216–219.
- Kellner, U., Wissinger, B., Tippmann, S., Kohl, S., Kraus, H., & Foerster, M. H. (2004). Blue cone monochromatism: Clinical findings in patients with mutations in the red/green opsin gene cluster. *Graefes Archive for Clinical and Experimental Ophthalmology*, *242*(9), 729–735.
- Ladekjaer-Mikkelsen, A.-S., Rosenberg, T., & Jørgensen, A. L. (1996). A new mechanism in blue cone monochromatism. *Human Genetics*, *98*, 403–408.
- Lewis, A., Williams, P., Lawrence, O., Wong, R. O. L., & Brockerhoff, S. E. (2010). Wild-type cone photoreceptors persist despite neighboring mutant cone degeneration. *The Journal of Neuroscience*, *30*(1), 382–389.
- Li, K. Y., & Roorda, A. (2007). Automated identification of cone photoreceptors in adaptive optics retinal images. *Journal of the Optical Society of America A*, *24*(5), 1358–1363.
- Linberg, K. A., & Fisher, S. K. (1990). A burst of differentiation in the outer posterior retina of the eleven-week human fetus: An ultrastructural study. *Visual Neuroscience*, *5*(1), 43–60.
- Marmor, M. F., Holder, G. E., Seeliger, M. W., & Yamamoto, S. (2004). Standard for clinical electroretinography (2004 update). *Documenta Ophthalmologica*, *108*, 107–114.
- Michaelides, M., Johnson, S., Simunovic, M. P., Bradshaw, K., Holder, G., Mollon, J. D., et al. (2005). Blue cone monochromatism: A phenotype and genotype assessment with evidence of progressive loss of cone function in older individuals. *Eye*, *19*(1), 2–10.
- Nathans, J., Davenport, C. M., Maumenee, I. H., Lewis, R. A., Hejtmancik, J. F., Litt, M., et al. (1989). Molecular genetics of human blue cone monochromacy. *Science*, *245*, 831–838.
- Nathans, J., Maumenee, I. A., Zrenner, E., Sadowski, B., Sharpe, L. T., Lewis, R. A., et al. (1993). Genetic heterogeneity among blue-cone monochromats. *American Journal of Human Genetics*, *53*, 987–1000.
- Neitz, M., Carroll, J., Renner, A., Knau, H., Werner, J. S., & Neitz, J. (2004). Variety of genotypes in males diagnosed as dichromatic on a conventional clinical anomaloscope. *Visual Neuroscience*, *21*, 205–216.
- Neitz, M., & Neitz, J. (2001). A new mass screening test for color-vision deficiencies in children. *Color Research and Application*, *26*, S239–S249.
- Pallikaris, A., Williams, D. R., & Hofer, H. (2003). The reflectance of single cones in the living human eye. *Investigative Ophthalmology and Visual Science*, *44*(10), 4580–4592.
- Provis, J. M., Diaz, C. M., & Dreher, B. (1998). Ontogeny of the primate fovea: A central issue in retinal development. *Progress in Neurobiology*, *54*(5), 549–580.
- Pum, D., Ahnelt, P. K., & Grasl, M. (1990). Iso-orientation areas in the foveal cone mosaic. *Visual Neuroscience*, *5*, 511–523.
- Putnam, N. M., Hofer, H. J., Doble, N., Chen, L., Carroll, J., & Williams, D. R. (2005). The locus of fixation and the foveal cone mosaic. *Journal of Vision*, *5*(7), 632–639.
- Rha, J., Dubis, A. M., Wagner-Schuman, M., Tait, D. M., Godara, P., Schroeder, B., et al. (2010). Spectral domain optical coherence tomography and adaptive optics: Imaging photoreceptor layer morphology to interpret preclinical phenotypes. In J. G. Hollyfield, R. E. Anderson, & M. M. LaVail (Eds.), *Retinal degenerative diseases* (pp. 309–316). Springer.
- Rha, J., Jonnal, R. S., Thorn, K. E., Qu, J., Zhang, Y., & Miller, D. T. (2006). Adaptive optics flood-illumination camera for high speed retinal imaging. *Optics Express*, *14*(10), 4552–4569.
- Rodieke, R. W. (1991). The density recovery profile: A method for the analysis of points in the plane applicable to retinal studies. *Visual Neuroscience*, *6*(2), 95–111.
- Rossi, E. A., & Roorda, A. (2010). The relationship between visual resolution and cone spacing in the human fovea. *Nature Neuroscience*, *13*(2), 156–157.
- Rossi, E. A., Weiser, P., Tarrant, J., & Roorda, A. (2007). Visual performance in emmetropia and low myopia after correction of high-order aberrations. *Journal of Vision*, *7*(8), 1–14.
- Sharp, A., Robinson, D., & Jacobs, P. (2000). Age- and tissue-specific variation of X chromosome inactivation ratios in normal women. *Human Genetics*, *107*(4), 343–349.
- Sjoberg, S. A., Neitz, M., Balding, S. D., & Neitz, J. (1998). L-cone pigment genes expressed in normal colour vision. *Vision Research*, *38*, 3213–3219.
- Smallwood, P. M., Wang, Y. S., & Nathans, J. (2002). Role of a locus control region in the mutually exclusive expression of human red and green cone pigment genes. *Proceedings of the National Academy of Sciences USA*, *99*(2), 1008–1011.
- Spivey, B. E., Pearlman, J. T., & Burian, H. M. (1964). Electroretinographic findings (including flicker) in carriers of congenital X-linked achromatopsia. *Documenta Ophthalmologica*, *18*, 367–375.
- Torti, C., Považay, B., Hofer, B., Unterhuber, A., Carroll, J., Ahnelt, P. K., et al. (2009). Adaptive optics optical coherence tomography at 120,000 depth scans/s for non-invasive cellular phenotyping of the living human retina. *Optics Express*, *17*(22), 19382–19400.
- Wang, Y., Smallwood, P. M., Cowan, M., Blesh, D., Lawler, A., & Nathans, J. (1999). Mutually exclusive expression of human red and green visual pigment-reporter transgenes occurs at high frequency in murine cone photoreceptors. *Proceedings of the National Academy of Sciences USA*, *96*(9), 5251–5256.
- Zhang, Y., Poonja, S., & Roorda, A. (2006). MEMS-based adaptive optics scanning laser ophthalmoscopy. *Optics Letters*, *31*(9), 1268–1270.
- Zhang, Y., & Roorda, A. (2006). Evaluating the lateral resolution of the adaptive optics scanning laser ophthalmoscope. *Journal of Biomedical Optics*, *11*(1), 014002.